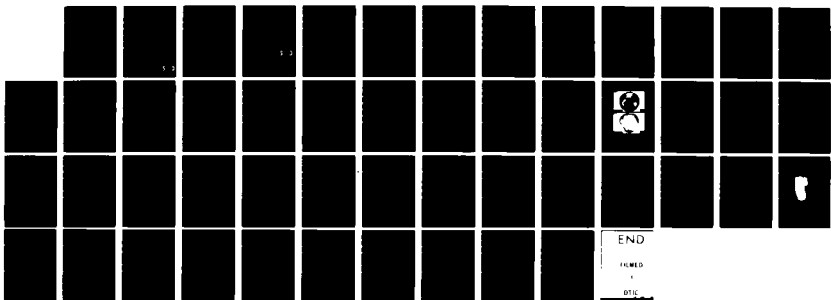
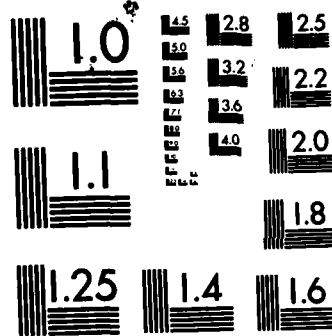


RD-A125 348 INP MATERIALS(U) MASSACHUSETTS INST OF TECH LEXINGTON 1/1  
LINCOLN LAB G W ISELER 30 SEP 82 ESD-TR-82-157  
F19628-80-C-0002

UNCLASSIFIED

F/G 28/2 NL





MICROCOPY RESOLUTION TEST CHART  
NATIONAL BUREAU OF STANDARDS-1963-A

A A 1 25348

ESD-TR-82-157

12

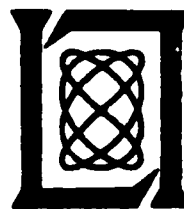
## Annual Technical Summary Report

InP Materials

30 September 1982

Prepared for the Department of the Air Force  
under Electronic Systems Division Contract F19628-80-C-0002 by

**Lincoln Laboratory**  
MASSACHUSETTS INSTITUTE OF TECHNOLOGY  
LEXINGTON, MASSACHUSETTS



Approved for public release; distribution unlimited.

88 03 07 03

B

DTIC  
ELECTE  
S MAR 7 1983 D

The work reported in this document was performed at Lincoln Laboratory, a center for research operated by Massachusetts Institute of Technology, with the support of the Department of the Air Force under Contract F19628-68-C-0002. A part of this support was provided by the Remote Air Development Center.

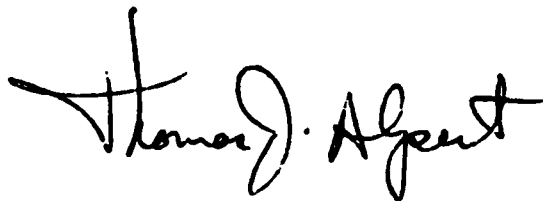
This report may be reproduced to satisfy needs of U.S. Government agencies.

The views and conclusions contained in this document are those of the contractor and should not be interpreted as necessarily representing the official policies, either expressed or implied, of the United States Government.

The Public Affairs Office has reviewed this report, and it is releasable to the National Technical Information Service, where it will be available to the general public, including foreign nationals.

This technical report has been reviewed and is approved for publication.

FOR THE COMMANDER



Thomas J. Alpert, Major, USAF  
Chief, ESD Lincoln Laboratory Project Office

**MASSACHUSETTS INSTITUTE OF TECHNOLOGY  
LINCOLN LABORATORY**

**InP MATERIALS**

**ANNUAL TECHNICAL SUMMARY REPORT  
TO THE  
ROME AIR DEVELOPMENT CENTER**

**1 OCTOBER 1981 — 30 SEPTEMBER 1982**

**ISSUED 12 JANUARY 1983**

**DTIC  
SELECTED  
S MAR 7 1983 D  
B**

**Approved for public release; distribution unlimited.**

**LEXINGTON**

**MASSACHUSETTS**

## ABSTRACT

↓

This report covers the work on InP materials carried out with support of the Department of the Air Force during the period 1 October 1981 through 30 September 1982. A part of this support was provided by the Rome Air Development Center. The current objectives of the program are to improve the yield of high-purity polycrystalline InP as source material for crystal growth and to optimize the liquid-encapsulated Czochralski (LEC) method in order to grow crystals with low dislocation density, low residual impurity concentration and uniform dopant concentration.

We have synthesized 30 ingots of InP with carrier mobilities at 77 K as high as  $8.2 \times 10^4 \text{ cm}^2\text{V}^{-1}\text{s}^{-1}$ . By using growth charges prepared by adding elemental In to the synthesized InP, we have pulled nominally undoped LEC boules with mobilities at 77 K as high as  $5.8 \times 10^4 \text{ cm}^2\text{V}^{-1}\text{s}^{-1}$ .

We have grown 35-mm-diameter LEC crystals with much reduced dislocation density, without Zn or S doping, by further increasing the thickness of the  $\text{B}_2\text{O}_3$  encapsulant layer to about 30 mm. Although this procedure significantly reduces the temperature gradients at the seed-melt interface, we have been able to obtain reproducible twin-free growth in the lower gradients by modifying the pulling rod pressure seal to reduce system vibration.

The prominent growth striations identified last year have been shown to persist even when the crucible containing the melt is immersed in liquid Ga to provide a more nearly isothermal melt environment.

Measurements of infrared transmission have been made on p-type InP samples to determine the free-carrier absorption due to holes. The absorption spectrum is found to be very similar to that reported for p-type GaP.

## INTRODUCTION

The goals of the InP materials program at Lincoln Laboratory are the development of reliable techniques for preparing high-quality InP single crystals of controlled electrical properties and the utilization of these techniques to produce crystals needed for research on optoelectronic devices such as GaInAsP/InP diode lasers and detectors.

Our program consists of two components: synthesis of InP from the elements and crystal growth by the liquid-encapsulated Czochralski (LEC) method. Synthesis, which is accomplished by directional solidification of In-rich solutions under controlled P pressure, is carried out in order to assure an adequate supply of polycrystalline charge material with the purity desired for LEC growth, since such material is not consistently available from commercial sources. In the area of LEC growth, by further reducing the temperature gradients in the vicinity of the seed-melt interface we have grown 35-mm-diam boules with significantly lower dislocation density. We have found that nominally undoped LEC crystals pulled from melts intentionally enriched with In exhibit electron concentrations of about  $10^{15}$  cm<sup>-3</sup> and 77 K mobilities approaching  $6 \times 10^4$  cm<sup>2</sup>-1s<sup>-1</sup>. We have continued to use x-ray topography and CO<sub>2</sub> laser transmission measurements to study the convection-induced growth striations in doped LEC crystals that are associated with abrupt changes in dopant concentration. These striations persist even when the crucible containing the melt is immersed in liquid Ga to provide a more nearly isothermal environment.



Classification	
By _____	
Distribution/ _____	
Availability Codes _____	
Dist	Avail and/or Special
A	

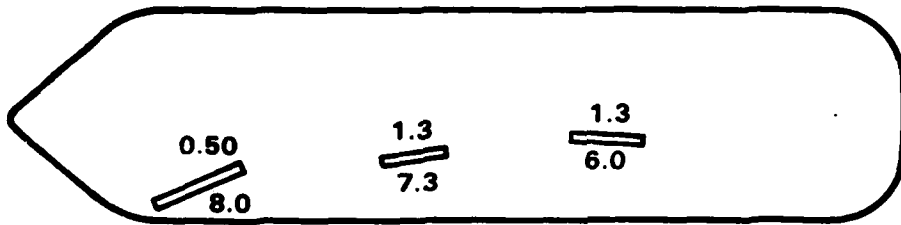
## SYNTHESIS

Synthesis of InP from the elements is carried out in fused silica ampoules, as described in the report for FY 81. During FY82, 30 ingots of polycrystalline InP each weighing about 900 g were synthesized. In order to characterize the polycrystalline material, Hall coefficient ( $R_H$ ) and resistivity ( $\rho$ ) measurements at 300 and 77 K were made when the grain size was large enough to permit rectangular single-crystal bars about  $10 \times 2 \times 1 \text{ mm}^3$  to be cut out. All such samples were n-type. The electron concentration at 300 K ( $n_{300}$ ) was calculated from the expression  $n = -1/eR_H$  (i.e., the Hall factor was assumed to be 1), and the Hall mobility at 77 K ( $\mu_{77}$ ) was calculated from  $\mu = R_H/\rho$ .

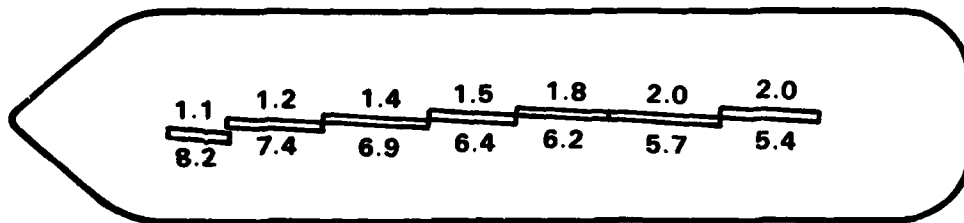
Seven bars for electrical characterization were cut from ingot 5 along its length at the positions indicated on the scale drawing shown in Fig. 1. The measured values of  $n_{300}$  increase monotonically from  $1.1 \times 10^{15} \text{ cm}^{-3}$  near the first-to-freeze end at the left of the diagram to  $2.0 \times 10^{15} \text{ cm}^{-3}$  near the last-to-freeze end, while  $\mu_{77}$  decreases from  $8.2 \times 10^4$  to  $5.4 \times 10^4 \text{ cm}^2\text{V}^{-1}\text{s}^{-1}$ . For three samples from a second ingot and two from a third, which were cut out at the positions shown in Fig. 1, the data indicate a similar variation in  $n_{300}$  and  $\mu_{77}$  with distance. The simultaneous increase in carrier concentration and decrease in mobility show that the shallow donor concentration systematically increases along the length of the ingots.

For 18 of the ingots synthesized in FY 82, electrical measurements were made on a sample cut from the region of each ingot between 1 and 3 inches from the first-to-freeze end, where the grain size was generally largest. Table 1 lists in chronological order the values of  $n_{300}$ , which range from  $5.0 \times 10^{14}$

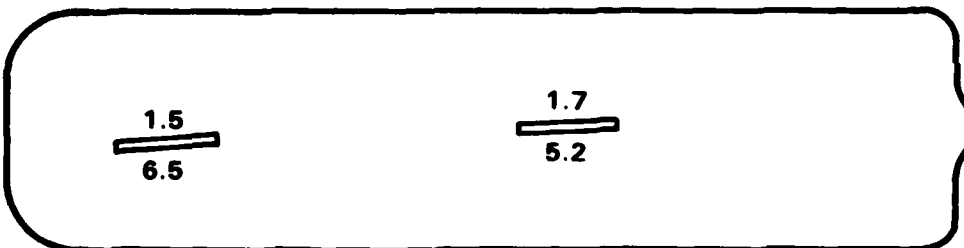
120861-N



INGOT 2



INGOT 3



INGOT 5

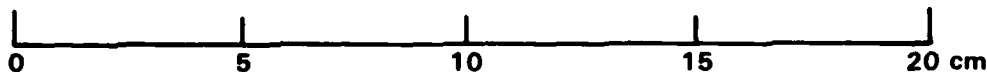


Fig. 1 Locations of samples cut for electrical characterization from three polycrystalline InP ingots. The values shown above and below each sample are the electron concentration at 300 K (in units of  $10^{15} \text{ cm}^{-3}$ ) and Hall mobility at 77 K (in units of  $10^4 \text{ cm}^2 \text{V}^{-1} \text{s}^{-1}$ ), respectively.

TABLE 1  
Synthesis parameters and electrical properties  
of polycrystalline InP ingots

Ingot	Indium			Phosphorus			InP (10 <sup>4</sup> cm <sup>2</sup> V <sup>-1</sup> s <sup>-1</sup> )
	(Source, 1 lot)	Vac. (°C., h)	Max. bake temp. (°C)	(Source, 1 lot)	Temp. (°C)	$\eta_{300}$ (10 <sup>13</sup> cm <sup>-3</sup> )	
1	MCP HR/68	--	1050	MCP 80/09	440	3.0	4.2
4	MCP HR/72	900, 16	1051	MCP 80/09	440	0.63	8.0
5	ICA 3243	900, 6	1048	MCP 80/09	444	1.1	8.2
7	MCP HRR/4	900, 6	1051	MCP 80/09	446	2.5	5.4
8	MCP HRR/4	--	1058	MCP 80/09	441	1.5	6.5
10	MCP HRR/2	900, 6	1056	MCP 80/08	443	1.7	5.6
11	MCP HR/72 HR/66 HR/68	900, 6	1053	MCP 81/01	440	0.96	4.7
13	MCP HRR/4	900, 6	1043	JM 84221	440	1.5	5.5
14	MCP HRR/4	900, 6	1051	MCP 80/02	441	1.5	6.0
16	MCP HRR/4	950, 8	1054	MCP 80/08	459	0.76	6.4
18	MCP HRR/5	900, 8	1051	MCP 81/02	470	1.6	5.1
19	MCP HRR/5	750, 12	1048	MCP 81/02	467	1.2	3.8
20	MCP HRR/5	850, 8	1045	MCP 81/02	445	0.88	5.4
22	MCP HRR/134	850, 6	1066	MCP 81/02	467	14.0	1.7

TABLE 1 (cont)

Ingot (lot)	Indium			Phosphorus		InP	
	(Source, Vac.)	Bake (°C, h)	Max. boat temp. (°C)	(Source, lot)	Temp. (°C)	$n_{300}$ ( $10^{13}$ cm $^{-3}$ )	$n_{77}$ ( $10^4$ cm $^2V^{-1}s^{-1}$ )
23	MCP HR/134	750, 7	1052	RASA 20320	474	160	0.37
24	MCP HR/134	750, 6	1070	MCP 82/01	471	6.4	2.8
25	MCP HR/134	750, 6	1052	RASA 20320	453	12.0	1.9
26	MCP HR/134	750, 6	1050	MCP 82/01	445	1.5	4.1

to  $1.6 \times 10^{17} \text{ cm}^{-3}$ , and the values of  $\mu_{77}$ , which range from  $3.7 \times 10^3$  to  $8.2 \times 10^4 \text{ cm}^2\text{V}^{-1}\text{s}^{-1}$ . Ten of the 18 values of  $\mu_{77}$  exceed  $5.0 \times 10^4 \text{ cm}^2\text{V}^{-1}\text{s}^{-1}$ . The high values of  $n_{300}$  and low values of  $\mu_{77}$  measured for some of the ingots are discussed below.

Figure 2 shows in histogram form the distribution of the  $\mu_{77}$  values measured for first-to-freeze samples from the ingots prepared in FY82 and also for such samples from the FY80 and FY 81 ingots. These  $\mu_{77}$  values are plotted vs the corresponding values of  $n_{77}$  in Fig. 3. The solid curves were calculated theoretically by Walukiewicz et al.<sup>1</sup> for values of the compensation ratio (ratio of ionized acceptor concentration  $N_A$  to ionized donor concentration  $N_D$ ) of 0, 0.2 and 0.4. Only one measured value of  $\mu_{77}$  lies more than 10% above the theoretical curve for no compensation. According to the curves, the compensation ratio is less than 0.4 for all but 4 of the 44 samples. Of the 23 samples with  $\mu_{77} > 5 \times 10^4 \text{ cm}^2\text{V}^{-1}\text{s}^{-1}$ , only 3 are compensated more than 20%, whereas 13 of the 21 remaining samples are compensated more than 20%. This difference may be partially due to our taking the Hall factor  $r$  equal to 1 in determining  $n_{77}$  and  $\mu_{77}$ . As reported below, we have found that  $r$  is actually about 1.14 for  $n \sim 10^{15} \text{ cm}^{-3}$ , and it is well known that  $r = 1$  for degenerate material.

In 1981 Kubota and Sugii<sup>2</sup> reported the synthesis of polycrystalline InP with  $\mu_{77} = 7.91 \times 10^4 \text{ cm}^2\text{V}^{-1}\text{s}^{-1}$  from an In charge that had been vacuum baked at 900°C for 6 h. In FY82, we have therefore baked most of the In charges for our synthesis runs in a high-temperature system evacuated with a vac-ion pump to a pressure of about  $10^{-6}$  Torr. For the 18 measured ingots, Table 1 lists the temperature and time of each In bake, the sources and lot numbers of the

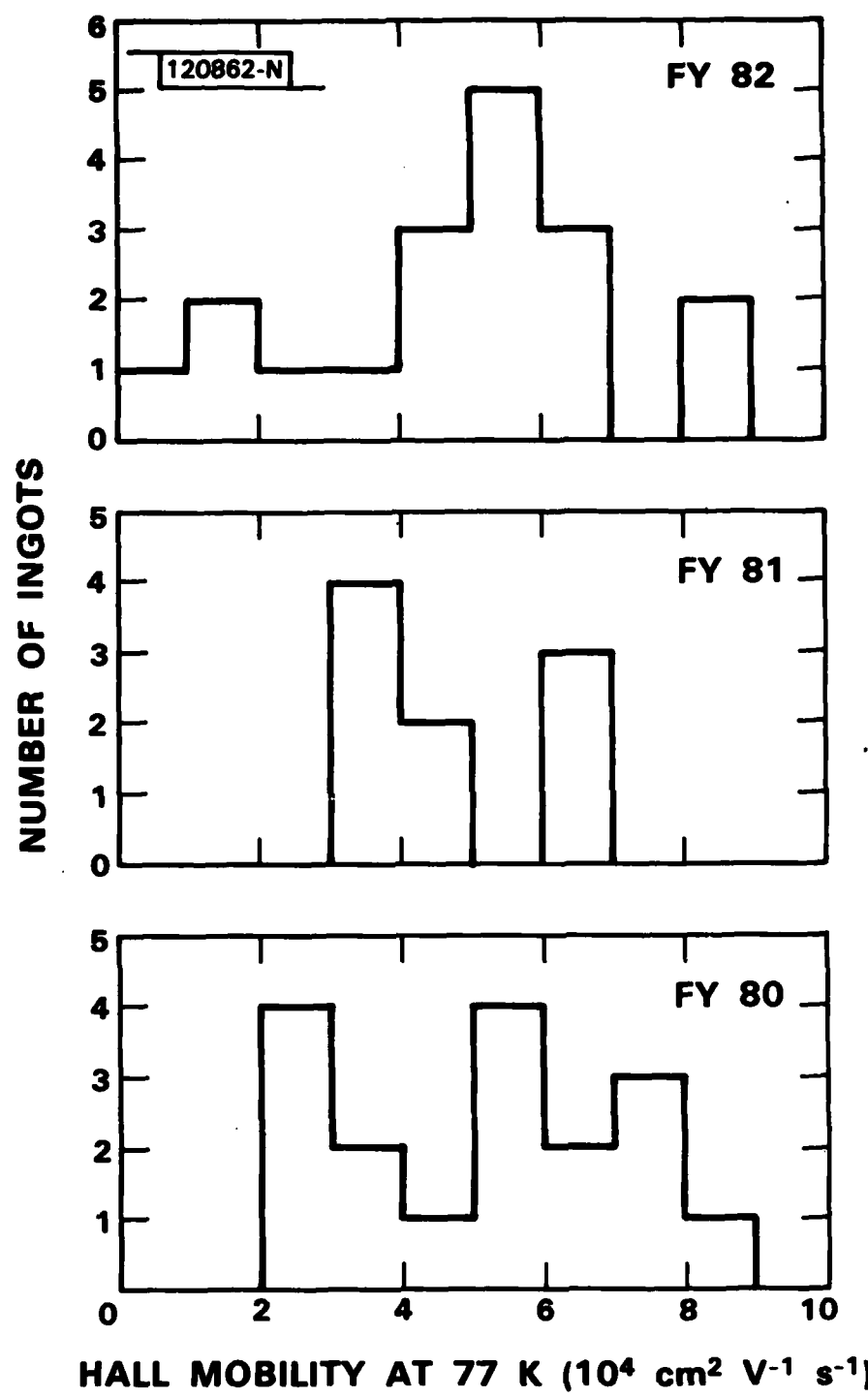


Fig. 2 Distribution of electron Hall mobilities at 77 K for polycrystalline InP ingots.

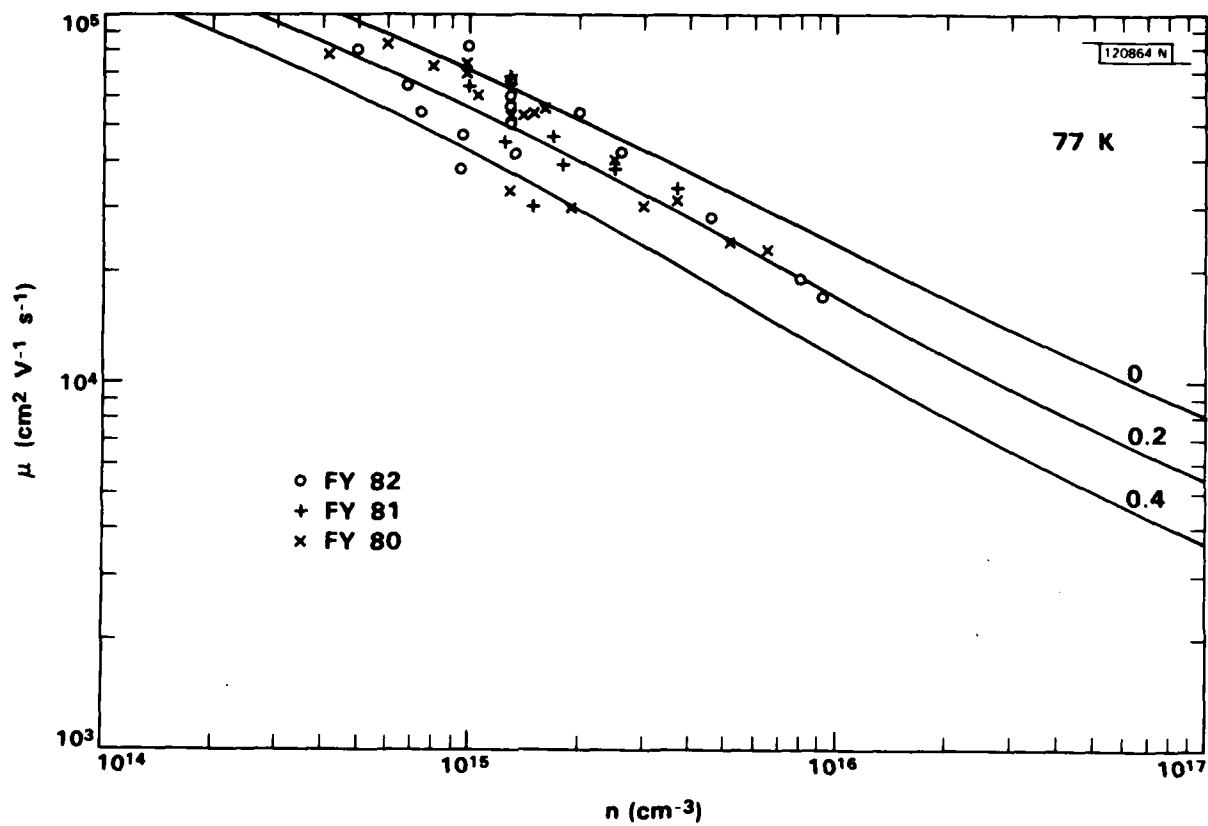


Fig. 3 Hall mobility vs electron concentration at 77 K for polycrystalline InP ingots. The solid curves were calculated for the indicated values of the compensation ratio.

In and P used as starting materials, the maximum temperature in the vicinity of the In boat, and the P reservoir temperature during the synthesis run. The highest mobilities measured in FY82 were exhibited by ingots 4 and 5, for which the In was vacuum baked. However, the results for ingots 7 and 8, which were made with In and P from the same lots, show that vacuum baking did not always improve the quality of the polycrystalline InP. The carrier concentration is slightly higher and the mobility lower for ingot 7, although the In for this ingot was baked while that for ingot 8 was not. It appears that some impurities which are electrically active in InP are inhomogeneously distributed within a particular lot of In or P or that some uncontrolled aspects of the synthesis technique can mask the effect of vacuum baking the In charge.

Examination of the data in Table 1 reveals a striking difference in electrical properties between the first 13 ingots (ingots 1 through 20) and the last 5. In the first group,  $n_{300}$  exceeds  $2 \times 10^{15} \text{ cm}^{-3}$  for only 2 ingots; in the second group,  $n_{300}$  is less than  $2 \times 10^{15} \text{ cm}^{-3}$  for only one ingot (the last) and ranges from  $6.4 \times 10^{15}$  to  $1.6 \times 10^{17} \text{ cm}^{-3}$  for the rest. In the first group, 10 ingots have values of  $\mu_{77}$  ranging from  $5.1$  to  $8.2 \times 10^4 \text{ cm}^2\text{V}^{-1}\text{s}^{-1}$ , and the lowest value is  $3.8 \times 10^4 \text{ cm}^2\text{V}^{-1}\text{s}^{-1}$ . In the second group, the highest value of  $\mu_{77}$  is only  $4.1 \times 10^4 \text{ cm}^2\text{V}^{-1}\text{s}^{-1}$  (for the last ingot), and the other values range from  $2.8 \times 10^4$  down to  $3.7 \times 10^3 \text{ cm}^2\text{V}^{-1}\text{s}^{-1}$ . These results show that the donor concentrations are much higher in the second group (except for the last ingot) than in the first. We believe that this difference is probably due to the presence of relatively high concentrations of impurities in the starting materials used for the second group. Note that

In from MCP lot HR/134 was used for all the ingots in this group and that P from RASA Industries was used for two of these ingots (including the one with by far the highest electron concentration), but neither of these materials was used for any of the ingots in the first group.

In an attempt to identify impurities in the starting materials that have a major effect on the electrical properties of the polycrystalline InP ingots, we used spark-source mass spectrography (SSMS) to analyze 7 samples of In from MCP lots HR/68, HRR/4 and HRR/5, which provided the In charges used for 9 of the first 13 InP ingots listed in Table 1. (Analysis of elemental P by SSMS is impractical.) Two of the samples from HRR/5 were vacuum baked before analysis. Because In adheres to the fused-silica boats in which it is baked, these samples were obtained by using special boats with the design shown schematically in Fig. 4. Each boat ended in a small-diameter, closed-end tube that was filled with molten In during the baking procedure because the vacuum furnace was tilted about 20° from the horizontal. After the system was cooled to room temperature the small tube was broken off, and the In sample to be analyzed was obtained by etching off the fused silica with HF. The boat was then sealed into the synthesis ampoule. During synthesis, surface tension prevented the loss of molten In through the small hole formed where the sample tube was broken off.

The results of the SSMS analyses are listed in Table 2, where the concentrations of the impurity elements detected in the In samples are given in parts per million atomic (ppma). For an element with a distribution coefficient of 1 in InP, a concentration of 1 ppma in In would yield a concentration of  $2 \times 10^{16} \text{ cm}^{-3}$  in the synthesized InP. In general, the

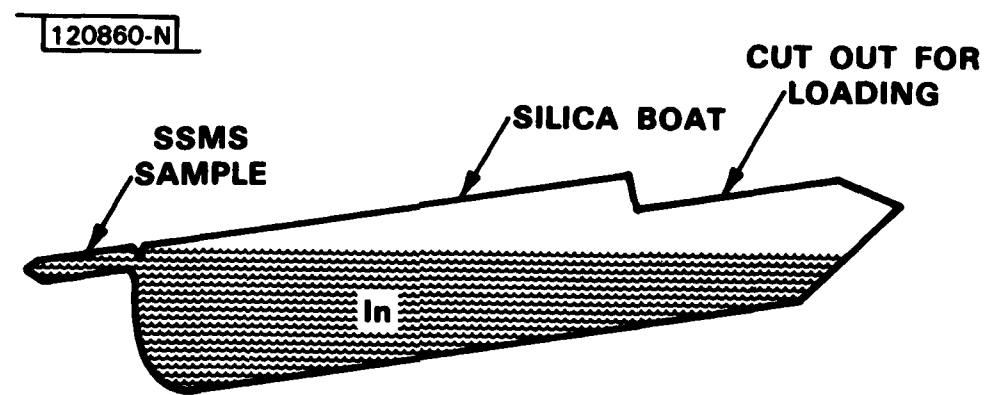


Fig. 4      Design of fused-silica boats used for obtaining vacuum-baked In samples for spark-source mass spectrographic (SSMS) analysis.

TABLE 2  
Spark-source mass spectrographic analyses of MCP In

Element	HR/68		HR/4		HR/5		
	As rec.	As Rec. #1	As rec. #2	As rec. #3	As rec.	Vac. baked <sup>a</sup>	Vac. baked <sup>b</sup>
Bi	0.08	0.2	0.07		0.03	4	0.3
Pb	0.2	0.4	0.07		0.08	0.3	0.3
Au	<0.2	<1	<0.8		<1	<1	<0.7
Ta	0.5	3	0.6	0.07	0.4	1	0.7
Ba					0.03		
Cs	<0.1		<0.03				
Sn	0.2	0.1			0.06		
Cd		0.08					
Zn			<0.04		<0.05	<0.02	<0.02
Cu	0.1	0.05	0.2	0.2	2	0.2	0.3
Ni	0.2	1	3	1	0.3	4	4
Fe	0.07	0.2	0.03	0.02	<0.2	0.03	0.03
Mn		0.02					
Cr		0.06	0.02		0.02	0.005	0.02
Ti		0.2					

TABLE 2 (cont)

Element	HR/68			HRR/4			HRR/5		
	As rec.	As Rec. #1	As rec. #2	As rec. #3	As rec.	Vac. baked <sup>a</sup>	Vac. baked <sup>b</sup>	As rec.	Vac. baked <sup>a</sup>
K	3	0.6	2	0.4	0.5	0.2	0.1		
Ca		0.1	0.04	0.02	0.04	0.01	0.01		
Cl	0.1		0.04	0.03	0.02	0.05	0.03		
S	0.1	<0.03	0.3	0.03	0.02	0.2	<0.1		
Si	0.5	11	10	10	0.3	0.05	0.03		
Al	1	2	2	0.2	0.2	0.05	0.03		
Mg	0.04	0.02	0.06	0.01	0.02	0.006	0.006		
F	0.06	0.4	0.1	0.04	0.08	0.2	0.2		
O	>40	10	>100	>100	0.4	0.2	0.4		
N	0.07	0.03	0.1	0.4	0.01	0.02	0.07		
C	0.3	0.3	0.7	>100	0.03	0.1	0.3		
B		0.04	0.5	0.4	0.01	0.1	0.4		
<u>Nominal</u>									
Detection Limit	0.03	0.01	0.03	0.015	0.02	0.006	0.006		

<sup>a</sup>Baked at 750°C for 12 h; charge used for ingot 19.  
<sup>b</sup>Baked at 850°C for 8 h; charge used for ingot 20.

reported concentrations should agree to within a factor of 3 with the true values; for a given element, the relative concentrations measured for the different samples should be much more accurate.

We have compared the results in Table 2 with those in Table 1 in order to investigate whether the concentrations found in the In samples of elements known to be shallow donor impurities in InP are correlated with the donor concentrations indicated by the electrical properties of the InP ingots. The only shallow donor impurities detected are Sn, S, and Si. Direct comparison can be made between the analytical results and the electrical data for 4 ingots: 1 (made from as-received HR/68); 8 (made from as-received HRR/4); 19 and 20 (made from the two vacuum-baked samples of HRR/5). On the basis of these limited comparisons, no correlation is apparent between the donor concentrations in the In samples and the InP ingots.

Silicon has been suspected to be the predominant donor impurity in nominally undoped InP. It is therefore of particular interest that ingot 8 has quite a low donor concentration (as shown by the rather low value of  $n_{300}$  and the high value of  $\mu_{77}$ ), although it was made from as-received HRR/4, all three samples of which had Si concentrations of 10 or 11 ppma, by far the highest measured. In fact, ingot 8 is comparable in donor concentration to ingots 19 and 20, which were made from vacuum-baked charges of HRR/5 that analysis showed to contain only 0.05 and 0.03 ppma Si, respectively, by far the lowest Si concentrations measured. Compared to the as-received sample of HRR/5, the two vacuum-baked samples had concentrations of Si and Cu about an order of magnitude lower, as well as significantly lower concentrations of K, Ca, Al and Mg, but their concentrations of Bi and Ni were an order of

magnitude higher and the concentrations of Pb, S, F, and C were significantly higher.

Although all 3 as-received samples of HRR/4 were found to contain about the same concentration of Si, many of the other impurities varied widely in concentration from sample to sample. For example, the concentrations of B, C, N, O, S, and Fe differed by at least an order of magnitude. Although for some elements the variation may have been due in part to differences in sample handling, it appears that many impurities were distributed inhomogeneously in the as-received In. If this is generally the case, the use of chemical analysis to select In charge material would not be very effective in increasing the purity of the polycrystalline InP produced.

#### LEC GROWTH

##### 1. Growth in reduced temperature gradients

During FY82 we have continued our investigation of the growth of InP crystals by the LEC method, with the objective of obtaining improved substrate material for epitaxial growth and device fabrication. In order to reduce the defect density, the LEC growth conditions were changed in several significant ways. Figure 5 is a scale drawing of the crystal growth assembly used for a large part of FY82. This assembly has been modified by increasing the height of the PBN crucible from 38 to 53 mm, which permits the use of thicker B<sub>2</sub>O<sub>3</sub> encapsulant layers, and incorporating a Mo radiation shield that rests on a silica ring at the top of the RF susceptor. The Mo shield is a flat disc, with a central hole 60 mm in diameter, that completely covers the top edge of the 68-mm-diameter crucible as well as the top of the susceptor. In addition,

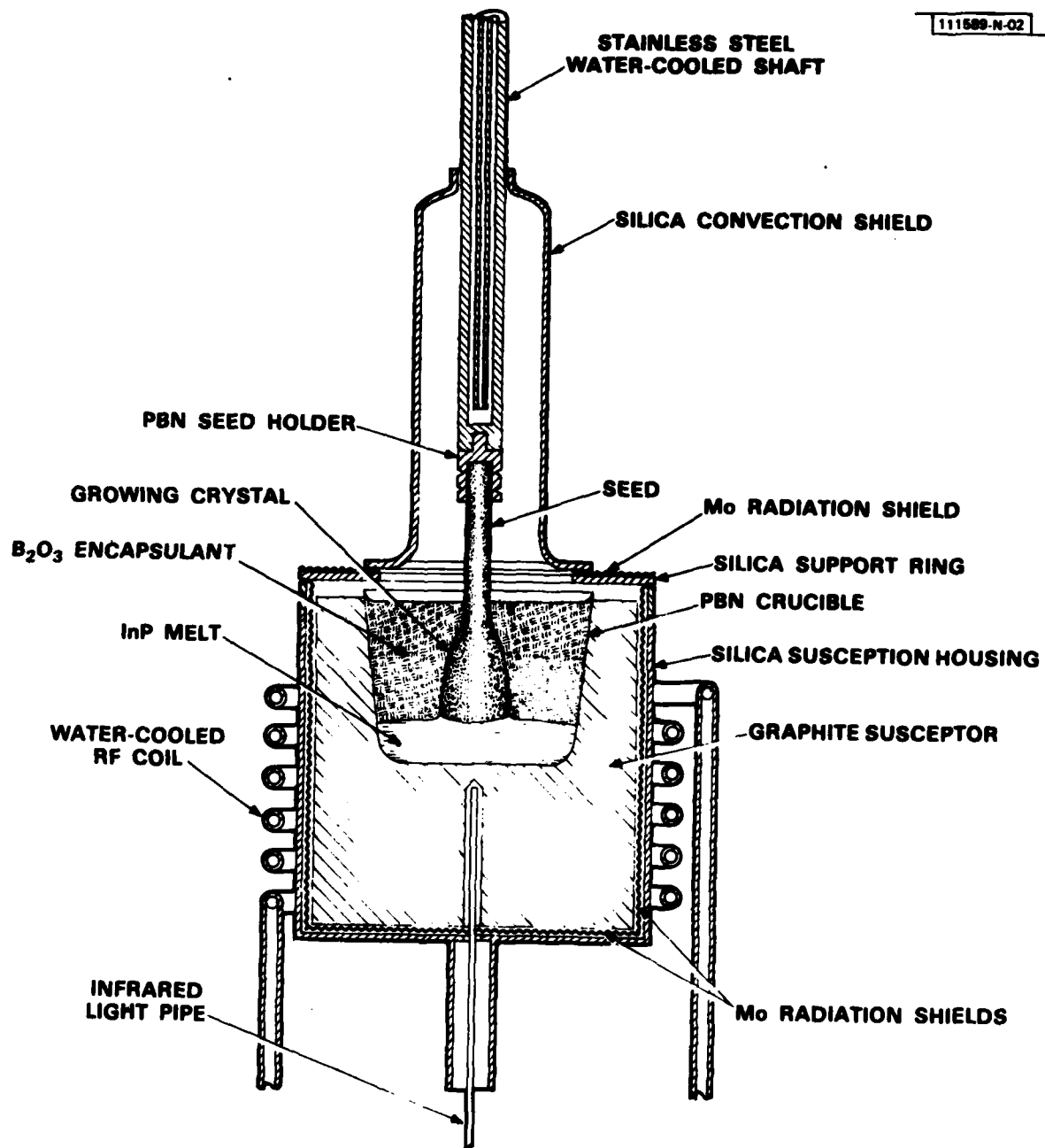


Fig. 5 Assembly for LEC growth of InP.

instead of soldering a relatively short InP seed to a Ni holder we now tie a longer seed with Mo wire to a PBN holder. (The crystals were grown in the (111) direction, with the (111)B face of the seed facing the melt.) All of these changes were made in an attempt to decrease the concentration of dislocations (which are generated due to thermally induced hoop stresses) by reducing the temperature gradients in the growing crystal. The upper Mo radiation shield enclosure reduces the heat losses from the top of the crucible due to radiation and to convection in the high-pressure Ar ambient. The heat losses from the crystal are therefore smaller both because the crucible walls are hotter and because the solid angle for radiation through the top is smaller.

The yield of twin-free, single-crystal boules under the modified conditions is surprisingly high, even when the thickness of the B<sub>2</sub>O<sub>3</sub> encapsulant layer exceeds 25 mm and there is nearly total runoff of the B<sub>2</sub>O<sub>3</sub> from the boule. We believe that this high yield, which was achieved in spite of using much lower temperature gradients at the crystal-melt interface, has been possible because we have further reduced vibration at the interface by replacing the spur gear drive on the crucible support shaft with a belt-driven crucible rotation mechanism.

Eight of 13 recent LEC growth runs with encapsulant layers thicker than 25 mm yielded entirely untwinned single crystal boules weighing about 250 g each, while 3 boules contained twins only near the lower end. The encapsulant layer thickness was measured at the center of the crucible after all of the InP charge had been pulled from the crucible. The boules were doped with either Fe, Sn, Cd, or S.

Three of the 13 boules were grown with encapsulant layers 31 mm thick. One of these boules (doped with Fe) was entirely untwinned, and the others (doped with Sn and Cd, respectively) were nearly so. All three have relatively low dislocation densities. Figure 6 shows an optical micrograph of the (111)B surface of a 35-mm-diameter wafer that was cut close to the bottom of the Fe-doped boule and etched with Huber solution<sup>3</sup> to produce dislocation etch pits. Figure 6 also shows a micrograph of a similarly etched wafer, only 24 mm in diameter, that was cut from the center of an earlier boule grown in a higher temperature gradient. The earlier wafer has a high density of etch pits that appear to be rather uniformly distributed; in typical regions we have measured values of  $3-4 \times 10^4 \text{ cm}^{-2}$ , although the highest values are in the range of  $1-2 \times 10^5 \text{ cm}^{-2}$ . The average etch pit density is much lower for the wafer from the boule grown with the thick encapsulant layer. The central region of this wafer is nearly free of dislocations, and most of the wafer has dislocation densities less than  $10^3 \text{ cm}^{-2}$ . The highest densities, which occur in three regions near the periphery, are about  $8 \times 10^4 \text{ cm}^{-2}$ . Substrates for epitaxial layers and for direct ion implantation taken from the low-dislocation regions of such wafers should prove useful in studies of the effects of dislocations on device performance.

We have investigated the possibility of using double-crystal x-ray diffraction to evaluate the crystalline perfection of InP, since Matsui, Watanabe and Seki<sup>4</sup> have reported that the width of rocking curves obtained by this technique exhibits a strong dependence on dislocation density. For diffraction from (400) planes, we have measured widths of about 10" (compared to the theoretical limit of 9.5" for perfect InP crystals) even for samples

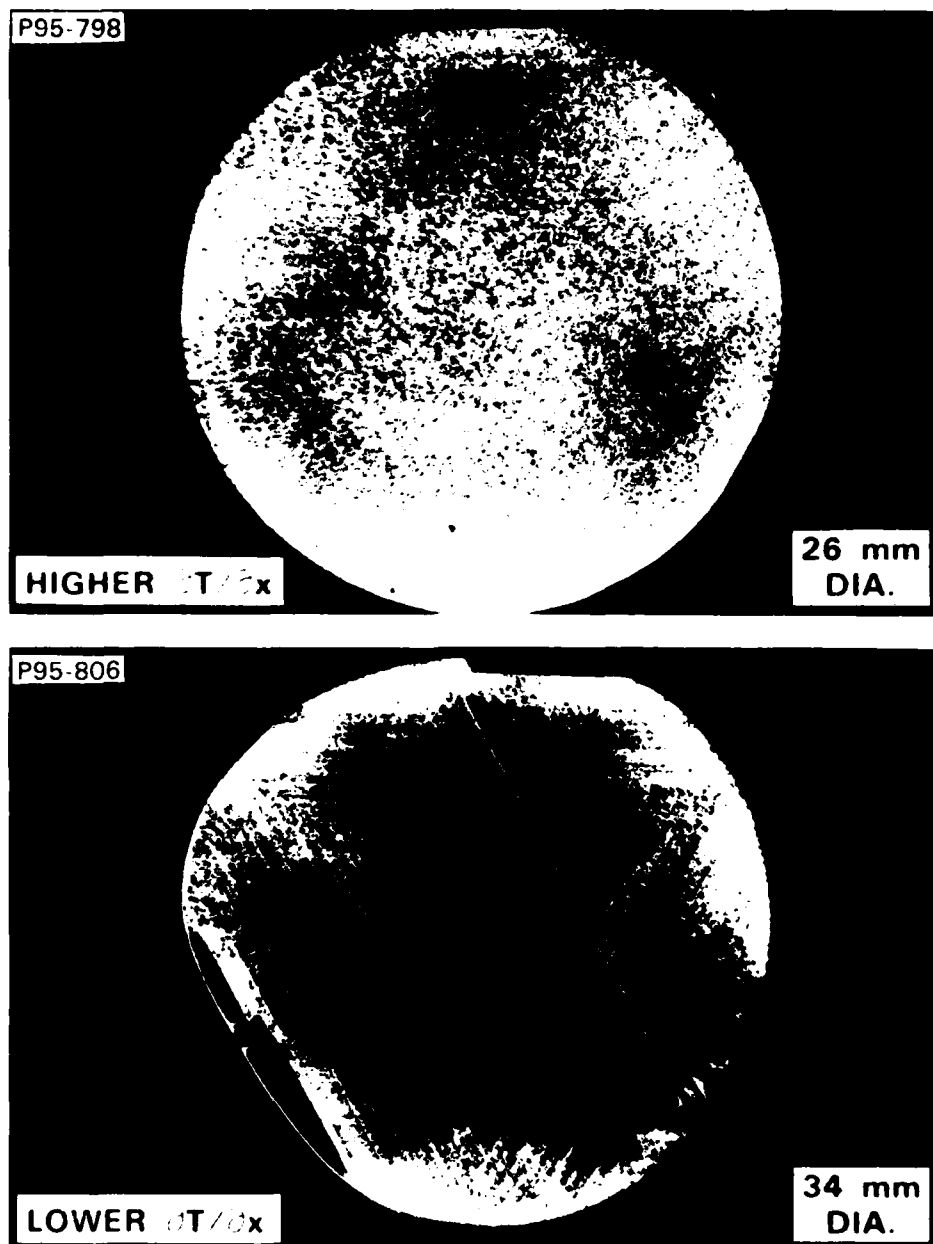


**Fig. 6** Optical micrographs showing dislocation etch pits in wafers cut from InP boules grown in higher (above) and lower (below) temperature gradients.

with etch pit densities greater than  $10^5$  cm $^{-2}$ . We have observed broader rocking curves only when surface damage was not entirely removed by etching. Therefore double-crystal diffraction is not a suitable technique for measuring the defect density in InP crystals. Etch pit studies and x-ray topography are currently the most reliable means for defect characterization.

## 2. Growth from In-rich melts

Our nominally undoped LEC boules have always exhibited higher values of  $n_{300}$  and lower values of  $\mu_{77}$  than the starting polycrystalline charges, which are solidified from In-rich melts. In an attempt to reduce the impurity concentration in such boules, we have investigated LEC growth from charges prepared by adding elemental In to polycrystalline ingot material. The boules grown from these charges exhibit a marked decrease in  $n_{300}$  and increase in  $\mu_{77}$  due to a reduction in donor concentration. In order to avoid constitutional supercooling during the growth of these boules, the temperature gradient in the melt was increased by removing the upper Mo radiation shield, using a thinner encapsulant layer, and increasing the ambient Ar pressure from 450 to 650 psi. The boules grown from In-rich charges, which we call "non-standard" boules, weigh from 100 to 200 g while the "standard" ones grown from charges without added In weigh from 250 to 300 g. The non-standard boules usually consist of 4 to 10 large grains, although we believe that a high yield of single-crystal boules could be grown from In-rich melts by optimizing the growth conditions, particularly the temperature gradient at the crystal-melt interface.

In the first experiments using In-rich melts, 3 boules were grown from charges in which the atom fraction of In ( $x$  in  $\text{In}_x\text{P}_{1-x}$ ) was nominally 0.56.

Two other boules were grown from charges with  $x = 0.59$  and  $0.52$ . The nominal values of  $x$  are calculated by taking the polycrystalline ingot material to be stoichiometric, with  $x = 0.5$ , although the ingots contain a small amount of metallic In occluded at grain boundaries. Table 3 lists the values of  $n_{300}$ ,  $n_{77}$ , and  $\mu_{77}$  found by resistivity and low-field Hall coefficient measurements on single-crystal samples cut from the first-to-freeze portions of these 5 non-standard boules, together with the corresponding values for the 2 standard boules grown just before them. (Values of the room-temperature mobility have not been tabulated, since these values are essentially the same for all the samples.) For the first 3 non-standard boules,  $n_{300}$  and  $n_{77}$  are considerably lower and  $\mu_{77}$  considerably higher than the values for the standard boules. Even the lowest  $\mu_{77}$  for these non-standard boules,  $4.2 \times 10^4 \text{ cm}^2\text{V}^{-1}\text{s}^{-1}$ , is equal to the highest value obtained for any of the more than 40 standard boules we have grown to date. The highest  $\mu_{77}$ ,  $5.7 \times 10^4 \text{ cm}^2\text{V}^{-1}\text{s}^{-1}$ , significantly exceeds the value of  $4.7 \times 10^4 \text{ cm}^2\text{V}^{-1}\text{s}^{-1}$  measured for the test sample cut from the polycrystalline ingot used to provide starting material. The fourth and fifth non-standard boules did not exhibit mobilities higher than those for the standard boules, probably because of inadvertent impurity contamination.

To make a more detailed study of the effect of melt composition, three successive growth runs were made using charge material from polycrystalline ingot 16, with In being added to the charges for the first and third runs. For the test sample cut near the first-to-freeze end of the ingot,  $n_{300}$  was  $7.6 \times 10^{14} \text{ cm}^{-3}$  and  $\mu_{77}$  was  $6.4 \times 10^4 \text{ cm}^2\text{V}^{-1}\text{s}^{-1}$ . In view of the usual increase in  $n_{77}$  and decrease in  $\mu_{77}$  with increasing distance from the

TABLE 3  
Electrical Properties of InP Boules

LEC boule	Melt composition (atom fraction In)	$n_{300}$ ( $10^{15} \text{ cm}^{-3}$ )	$n_{77}$ ( $10^{15} \text{ cm}^{-3}$ )	$(10^4 \text{ cm}^2 \text{V}^{-1} \text{s}^{-1})$
442	0.5	4.9	3.8	3.1
449	.5	4.5	3.9	3.5
452	.56	2.7	2.0	5.7
454	.56	2.5	2.3	4.2
455	.56	2.9	2.5	4.6
457	.59	6.1	4.7	3.0
461	.52	3.8	3.1	3.1

first-to-freeze end, the ingot was cut into three side-by-side longitudinal sections, and one section was used for each LEC run. After completion of each run, samples for electrical measurements were cut near the top, middle and bottom of the boule. For the two non-standard boules, the melt composition corresponding to each sample location was calculated from the weights of the polycrystalline charge material, the In added to the charge, and the portion of the boule that had solidified, taking both the polycrystalline material and the grown boule to be stoichiometric.

The results for the three additional boules, which are given in Table 4, confirm the dependence of electrical properties on melt composition found for the first three runs from the In-rich melts. All the values of  $n_{300}$  and  $n_{77}$  are much lower and all the values of  $\mu_{77}$  much higher for the non-standard boules than for the standard boule. Furthermore, the carrier concentrations decrease and the mobility increases from the top to the bottom of the non-standard boules (except that  $n_{77}$  is slightly lower for the middle sample of boule 470 than for the top sample). This variation can be attributed to the increase in the In content of the melt as the boule solidifies, since the opposite variation in carrier concentration and mobility is exhibited by the standard boule and by all other standard boules for which we have data. The variation along a standard boule occurs because impurities with distribution coefficients of less than unity segregate toward the bottom of the boule.

After the series of LEC runs just described, 4 more non-standard boules were grown. Electrical data for these boules are shown in Table 5. For 3 of the 4, the values of  $\mu_{77}$  are greater than those for any of the standard boules.

TABLE 4  
Electrical properties of InP boules grown from same charge material

Boule	Sample	Melt composition (atom fraction In)	$n_{300}$ ( $10^{15} \text{ cm}^{-3}$ )	$n_{77}$ ( $10^{15} \text{ cm}^{-3}$ )	$\mu_{77}$ ( $10^4 \text{ cm}^2 \text{V}^{-1} \text{s}^{-1}$ )
470	T	0.58	2.5	2.2	4.9
	M	.62	2.5	2.1	4.8
	B	.65	2.0	1.7	5.6
471	T	.5	4.9	4.0	3.2
	M	.5	5.4	4.1	2.8
	B	.5	6.1	4.8	2.7
472	T	.61	2.4	1.9	4.1
	M	.65	1.7	1.5	5.1
	B	.67	1.6	1.3	5.5

TABLE 5  
Electrical properties of InP boules

Boule	Sample	Melt composition (atom fraction In)	$n_{300}$ ( $10^{15} \text{ cm}^{-3}$ )	$n_{77}$ ( $10^{15} \text{ cm}^{-3}$ )	$\mu_{77}$ ( $10^4 \text{ cm}^2 \text{V}^{-1} \text{s}^{-1}$ )
474	T	.60	2.5	1.9	4.8
	B		1.7	1.4	5.8
477	T	.53	4.7	3.7	3.6
	B		6.9	4.6	3.1
480	T	.56	3.2	2.7	4.3
	B		2.4	2.1	5.0
494	T	.58	4.3	3.0	4.4
	B		3.8	2.7	4.3

In summary, of the 11 boules grown from In-rich solutions, 8 have exhibited mobilities superior to the best of the standard boules, and 2 of the other 3 were grown from charges with  $x$  of only 0.52 or 0.53. The maximum value of  $\mu_{77}$  measured to date for a non-standard boule is  $5.8 \times 10^4 \text{ cm}^2 \text{V}^{-1}\text{s}^{-1}$ , compared to the maximum reported value of  $5.3 \times 10^4 \text{ cm}^2\text{V}^{-1}\text{s}^{-1}$  for any LEC InP crystal.<sup>5</sup>

Over the past several years, we have observed a general increase in  $n_{300}$  (and  $n_{77}$ ) and an accompanying decrease in  $\mu_{77}$  for the nominally undoped standard boules. For example, boules 343 and 348 grown in FY81 each exhibit electron concentrations of  $2.9 \times 10^{15} \text{ cm}^{-3}$  and mobilities of 4.1 and  $4.2 \times 10^4 \text{ cm}^2\text{V}^{-1}\text{s}^{-1}$ , respectively, whereas boules 442 and 449 grown in FY82 exhibit electron concentrations of 4.9 and  $4.5 \times 10^{15} \text{ cm}^{-3}$ , respectively, and mobilities of 3.1 and  $3.5 \times 10^4 \text{ cm}^2\text{V}^{-1}\text{s}^{-1}$ , respectively. This apparent trend may be due at least in part to the fact that the more recent polycrystalline starting charges contain a smaller amount of occluded elemental In than those synthesized earlier.

In attempting to find an explanation for the difference in electrical properties between the non-standard and standard LEC boules, we have investigated the possibility that the values of  $R_H$  measured at low fields for the non-standard boules are anomalously high (i.e.,  $R_H > 1/ne$ ) because these boules contain metallic In inclusions incorporated during their growth from the In-rich melts. For GaAs, it has been found that Ga inclusions can result in such anomalous  $R_H$  values, in which case the magnetic field dependence of  $R_H$  is also anomalous.<sup>6</sup> We have therefore measured  $R_H$  at room temperature as a function of field for samples from both non-standard and standard boules. The

results for one sample of each type are shown in Fig. 7, where the ratio of  $R_H$  at each field to  $R_H$  at 15 T is plotted against field. Results are also shown for the sample from ingot 5 listed in Table 1 ( $\mu_{77} = 8.2 \times 10^4 \text{ cm}^2 \text{ V}^{-1}\text{s}^{-1}$ ) and for a sample supplied by RADC, which probably contains In inclusions.

The three upper curves in Fig. 7, which are almost identical, have the form characteristic of a homogeneous semiconductor, while the RADC sample has the form reported<sup>6</sup> for a semiconductor with metallic inclusions. We conclude that the improvement in the electrical properties of the non-standard boules is not due to measurement anomalies resulting from the presence of In inclusions. Consistent with this conclusion, in using an infrared microscope with a resolution of several micrometers to examine samples from these boules we have failed to find any opaque areas. (We also conclude that the electrical measurements on samples from our InP ingots are not significantly affected by In inclusions.)

Measurements of infrared transmission at 11.9  $\mu\text{m}$  for 3 samples from non-standard boules and 6 samples from standard boules also indicate that the low-field Hall measurements provide a good measure of the free carrier concentration for the non-standard boules. Since the absorption coefficient  $\alpha$  at this wavelength varies from about 0.1 to 1  $\text{cm}^{-1}$  for InP with electron concentrations in the  $10^{15}$  to  $10^{16} \text{ cm}^{-3}$  range, samples of the order of 1 cm thick are necessary for accurate absorption measurements. Because InP has a high refractive index, if a focused light beam were used the location of the focal point would be changed by the introduction of such thick samples into the optical path. To avoid errors due to this effect, the measurements were made with nearly parallel light from an off-axis parabolic mirror that was

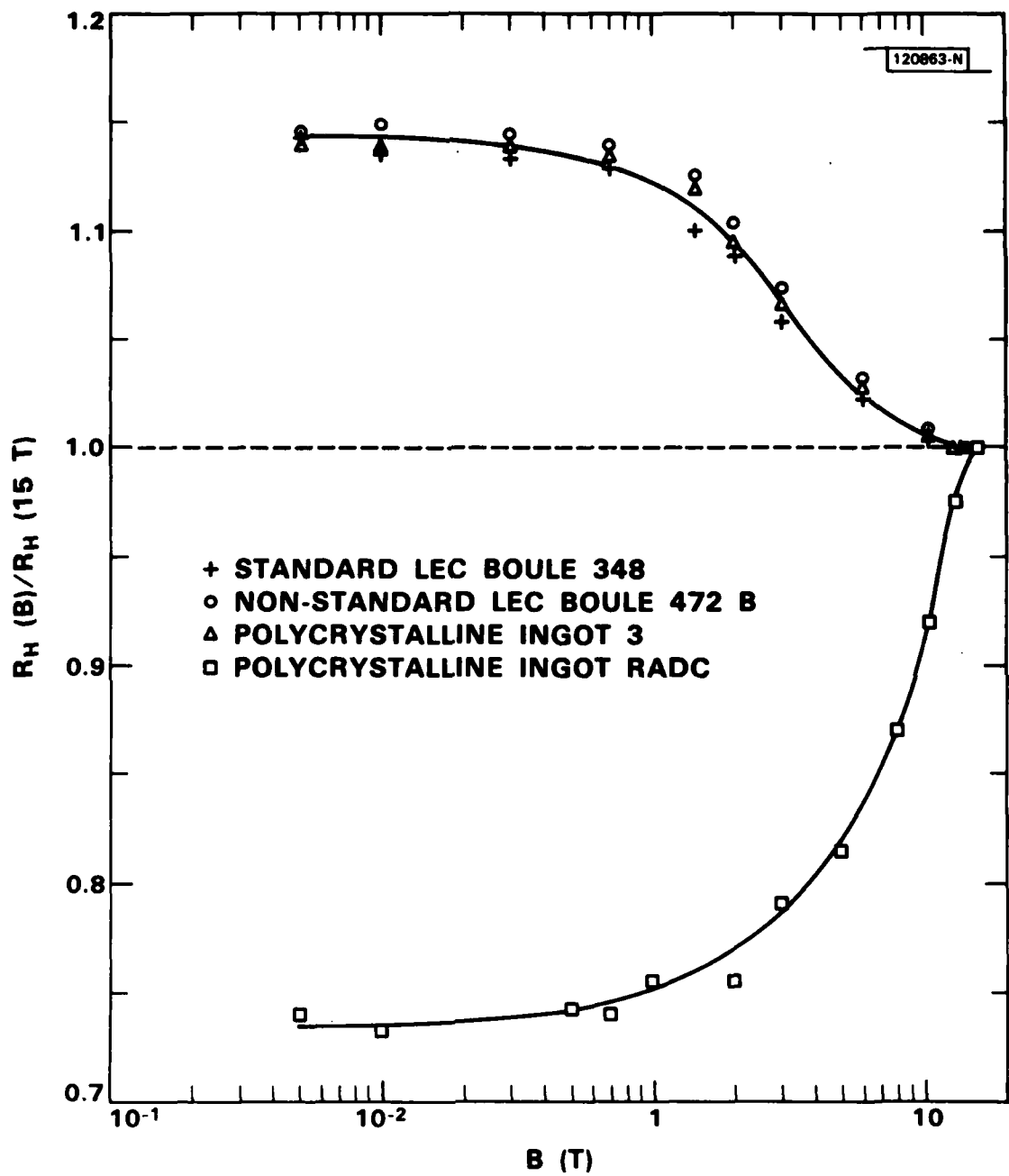


Fig. 7 Ratio of Hall coefficient at field  $B$  to Hall coefficient at 15 T vs  $B$  for InP samples at room temperature.

passed through an interference filter (bandpass of  $0.27\mu\text{m}$  centered at  $11.9\mu\text{m}$ ) and then through the sample, after which the transmitted radiation was detected by a pyroelectric element (active area of  $2\text{ mm}^2$ ) placed directly behind the sample. The absorption coefficient was calculated from the expression  $I/I_0 = [(1-R)^2 \exp(-\alpha x)] / [1-R^2 \exp(-2\alpha x)]$ , where  $I$  is the intensity transmitted through the sample,  $I_0$  is the intensity without the sample in the beam,  $x$  is the sample thickness and  $R$  is the reflectivity, taken as 0.256 at  $11.9\mu\text{m}$ .<sup>7</sup>

In Fig. 8 the values of  $\alpha$  deduced from the transmission data are plotted vs  $n_{300}$ . The dashed curve shown in the figure is the theoretical curve for  $11.9\mu\text{m}$  obtained by using the wavelength dependence given by Walukiewicz et al.<sup>1</sup> to adjust the values of  $\alpha$  calculated by those authors for  $10\mu\text{m}$ . The agreement between experiment and theory is remarkably good. Furthermore, the cross section for free-carrier absorption,  $\alpha/n_{300}$ , is the same within experimental error for the 3 samples from non-standard boules as for the 6 samples from standard boules. If the values of  $R_H$  measured for the non-standard samples were anomalously high because of the presence of In inclusions, the resulting reduction in  $n_{300}$  would make the measured values of  $\alpha/n_{300}$  higher than the true values. In addition, any infrared absorption or scattering by the opaque In inclusions would also increase  $\alpha/n_{300}$ , since it would reduce the transmission and consequently increase  $\alpha$ . The observed agreement between the cross section values for the non-standard and standard samples thus confirms the absence of measurements anomalies due to In inclusions. (Note that the lowest value of  $n_{300}$  in Fig. 8 was obtained for a standard sample, which was cut from boule 400.) This boule was found by SSMS

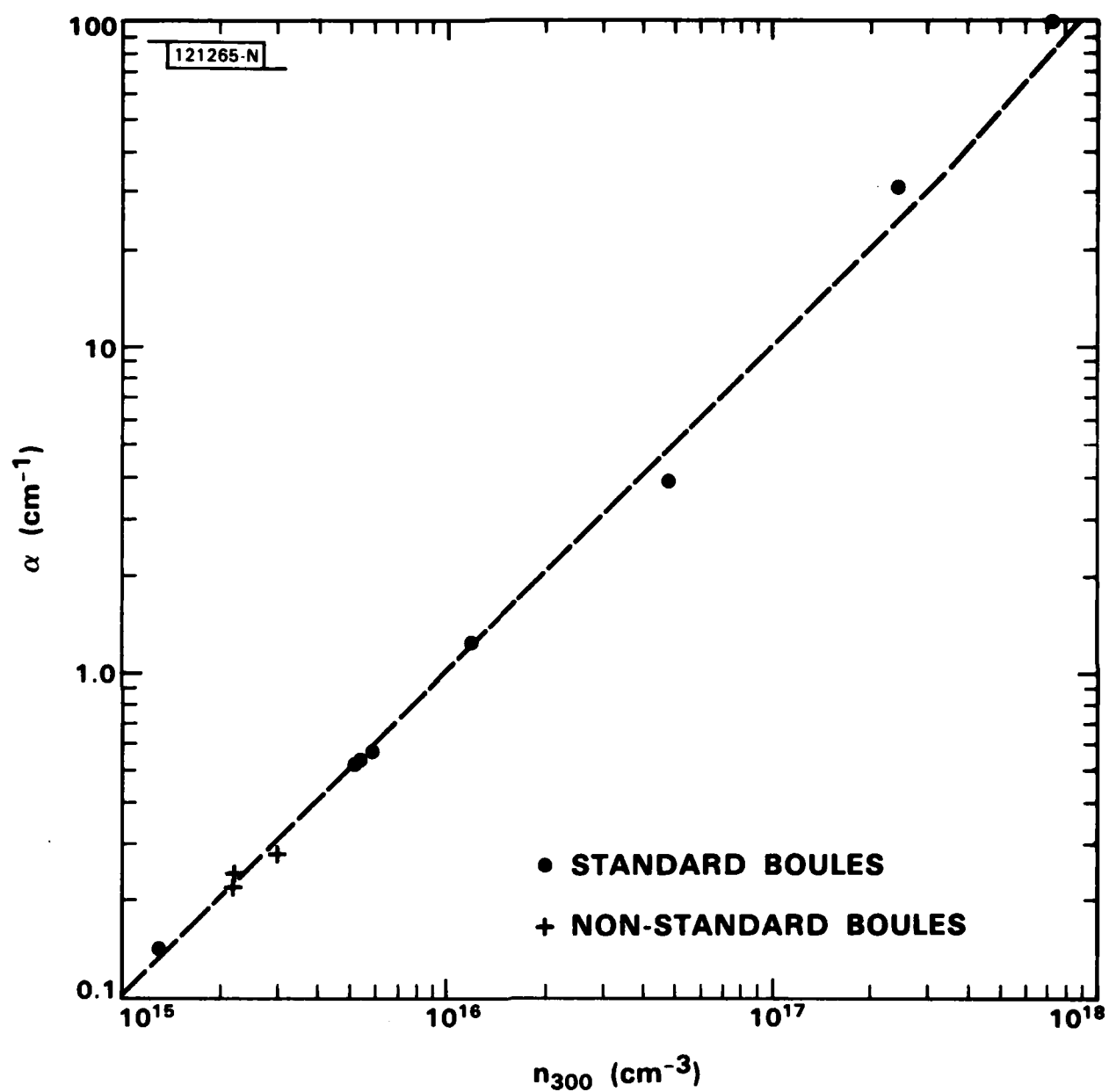


Fig. 8 Absorption coefficient at  $11.9 \mu\text{m}$  vs electron concentration at 300 K for InP samples from standard and non-standard boules. The dashed line is based on the theoretical calculations of Walukiewicz et al. (Ref. 1).

to contain a sufficient concentration of the shallow acceptor Zn to account for the reduction in  $n_{300}$ , which was accompanied by a reduction in  $\mu_{77}$  to  $1.2 \times 10^4 \text{ cm}^2\text{V}^{-1}\text{s}^{-1}$ .)

The reduction in carrier concentration and increase in mobility for the non-standard boules can therefore be attributed to a change in the concentration of electrically active centers -- in particular, to a reduction in the concentration of shallow donors. (The degree of acceptor compensation is so low in both standard and non-standard boules that the change in acceptor concentration, if any, cannot be determined from the electrical data.) The identity of the donor or donors associated with the change in electrical properties has not been established. One possibility is the native antisite defect consisting of a P atom located on an In site, whose concentration will be reduced by growth from an In-rich melt. The other principal possibility is an impurity, such as Si, that is a donor when located on an In site.

An SSMS investigation was undertaken in an attempt to identify the donor (and perhaps acceptor) impurities that have a major effect on the electrical properties of the nominally undoped boules. Table 6 shows the SSMS results, together with the values of  $n_{300}$  and  $\mu_{77}$ , for 12 samples taken from 7 boules, which are listed in chronological order. The concentrations of the impurities detected are reported in parts per million atomic relative to In; 1 ppma is equivalent to  $2 \times 10^{16} \text{ cm}^{-3}$  in InP.

The first sample listed in Table 6, which was taken from boule 400, was found to contain Zn at a concentration of  $1 \times 10^{16} \text{ cm}^{-3}$ . As noted above in discussing the infrared absorption measurements on another sample from this boule, this concentration of Zn accounts for the low values obtained for both

TABLE 6  
Spark-source mass spectrographic analyses of InP boules

Sample	400	429T	42981	42982	430T	4308	436B	442T	470T	4708	472T	4728
$n_{300}$ (10 <sup>15</sup> cm <sup>-3</sup> )	1.0	11	180	180	7.0	7.0	5.4	3.8	2.5	2.0	2.4	1.6
$n_{77}$ (10 <sup>4</sup> cm <sup>2</sup> V <sup>-1</sup> s <sup>-1</sup> )	1.2	1.9	0.29	0.29	2.8	2.7	2.9	3.1	4.9	5.6	4.1	5.5
Pb										0.08		
Ta	<0.1	0.04	0.04	0.7	<0.3				0.03	0.3	0.05	
Tb		<0.3	<0.3	<0.1					<0.02		<0.05	
Cs		<0.1	<0.3	<0.3	<0.1	<0.3				0.2		
Br											0.6	
Ni											0.5	
Fe						0.08					0.03	
Zn						0.5						
Cu						<0.2		<0.07	<0.07	<0.02	0.05	<0.02
Cr						0.02	0.05					
Ca						0.03	0.02	0.3	0.02		0.02	0.02
K						0.06	0.2	0.3	3	6	0.08	0.4
Cl						0.3	0.4	0.3	0.03	0.07	0.04	0.4
									0.1	0.1	1	0.007

TABLE 6 (cont)

Sample	400	429T	42981	42982	430T	4308	436B	442T	470T	4708	472T	472B
S	<1	<0.4	<0.4	<0.1	<0.4	<0.4	<0.4	<0.4	<0.09	<0.1	<0.1	<0.1
Si	0.1	2	0.6	to 0.4	<0.03	0.02	0.02	0.02	0.02	0.03	0.02	
Al	0.05	0.03	2		0.02			0.01	0.01	0.02	0.01	0.2
Mg		0.03	0.04									
F	0.08	0.04	0.2		0.01	0.08	0.2	0.003		0.004	0.02	
O	20	3	40	1	15	0.08	10.4	1	0.04	50	0.2	0.04
N	0.1	0.4	0.7	0.4	0.07			0.02	0.07	0.4	0.07	
C	20	50	60	0.7	70	0.03	1	10	0.06	4	0.2	0.07
B	1	0.3	7	3	0.04	0.01	0.1	0.2	25	0.04	0.1	
<hr/>												
Nominal Detection Limit	0.1	0.03	0.03	0.01	0.03	0.03	0.007	0.02	0.01	0.01	0.01	0.01

$n_{300}$  and  $\mu_{77}$ . The shallow donor impurity or impurities responsible for making the boule n-type were not detected by SSMS. However, S could have been present at a higher concentration than Zn without being detected, since the detection limit was significantly higher for S than for the other elements.

The next 5 samples listed in Table 6 were taken from boules 429 and 430, both of which were grown from nominally stoichiometric melts in fused silica crucibles. For all these samples the values of  $n_{300}$  are higher than those for boules grown from melts in PBN crucibles. It is probable that Si is the donor impurity responsible for the increase in carrier concentration. This is almost certainly the case for samples 429B1 and 429B2, for which  $n_{300}$  is  $1.8 \times 10^{17} \text{ cm}^{-3}$ . Although the measured Si concentrations are much higher for these two samples than for any of the others analyzed, their measured concentrations are much less than  $1.8 \times 10^{17} \text{ cm}^{-3}$ . The ratios of Si concentration to  $n_{300}$  are 0.22 and 0.067, respectively. These ratios not only indicate that in the SSMS analysis of InP the sensitivity is much lower for Si than for In; more important, the large difference between them shows that even the relative values of Si concentration are unreliable. The data for the other samples are consistent with these conclusions. Thus SSMS does not appear to be a satisfactory technique for determining Si in InP.

The remaining samples listed in Table 6 were taken from two standard boules (436 and 442) and from two non-standard boules (470 and 472), all grown from melts in PBN crucibles. No correlation between their measured impurity concentrations and electrical properties is apparent. For example, although sample 470B has the highest value of  $\mu_{77}$ , with a few exceptions its measured impurity concentrations are higher than those of the other non-standard

samples. Overall, these and the other results listed in Table 6 indicate that SSMS analysis is not a useful method for characterizing our nominally undoped LEC boules.

### 3. Growth Striations

As discussed in our FY81 report, we have shown by x-ray topography and scanning CO<sub>2</sub> laser transmission measurements that our intentionally doped LEC boules exhibit prominent growth striations associated with large variations in the doping concentration. Since these striations are very probably due to random convection currents caused by large temperature gradients in the melt, in order to minimize the striations we have made an attempt to establish growth conditions that would reduce these gradients. With this aim, in one growth run the graphite susceptor was replaced by a liquid Ga susceptor, and the PBN crucible containing the InP melt was immersed directly in the liquid metal. The Ga was held in a silica container fitted with integral silica tabs to keep the buoyant PBN crucible centered and immersed. To prevent rapid evaporation of the Ga, it was encapsulated with a thin layer of B<sub>2</sub>O<sub>3</sub>. The nominally stoichiometric InP melt, which was doped with Sn, was encapsulated with a layer of B<sub>2</sub>O<sub>3</sub> ~25 mm deep. By using the standard growth procedure we obtained a boule weighing 285 g that was largely untwinned. An x-ray transmission topograph of a (110) longitudinal sample from this boule is shown in Fig. 9. Random growth striations are still clearly visible. The variation in carrier concentration across the striations is indicated in Fig. 10, which is a recorder trace showing the intensity of transmitted CO<sub>2</sub> laser radiation versus distance along a vertical (111) direction for another (110) longitudinal slice. The values of  $n_{300}$  determined from the transmission data

P95-787

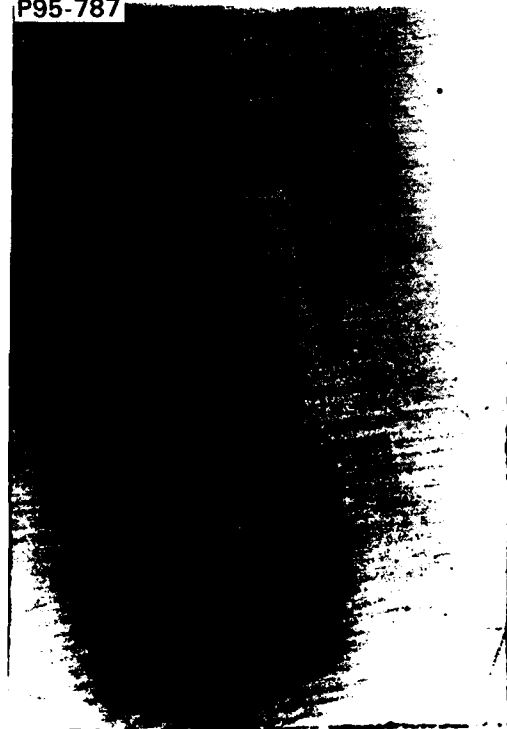


**Fig. 9** X-ray topograph of (110) longitudinal sample from Sn-doped LEC InP crystal.

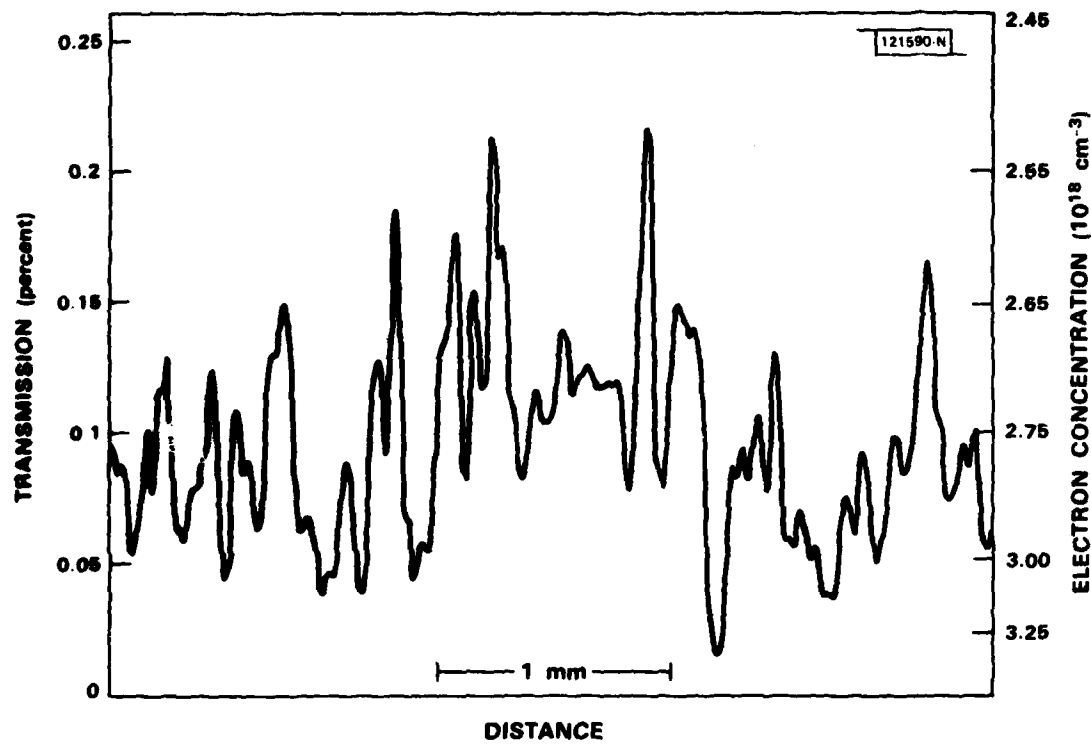


Fig. 10 Recorder trace showing transmission of  $\text{CO}_2$  laser radiation vs distance along vertical direction for Sn-doped LEC InP crystal.

vary from  $2.5$  to  $3.3 \times 10^{18} \text{ cm}^{-3}$  for this particular scan, and it is not unusual to find a variation of 15% over a  $100 \mu\text{m}$  distance. Since the growth striations were not dramatically changed by using the liquid Ga susceptor, and because the  $\text{B}_2\text{O}_3$  encapsulating the Ga broke the silica container upon solidifying, no further experiments of this type are planned.

Another approach to the problem of the growth striations is to reduce the effect of convection currents by stirring the melt more vigorously in order to decrease the thickness of the boundary layer at the crystal-melt interface. Experiments have been undertaken to study how the striations are affected by increasing the rates of seed and crucible rotation.

#### FREE-CARRIER ABSORPTION IN p-TYPE InP

Since no data had been published on the free-carrier absorption of p-type InP, in FY81 we began a series of measurements to determine the optical absorption coefficient  $\alpha$  at  $10.6 \mu\text{m}$  as a function of hole concentration, in order to obtain carrier concentration profiles from scanning  $\text{CO}_2$  laser absorption data for Zn- and Cd-doped crystals. These measurements have now been completed. Measurements have also been made of  $\alpha$  at  $1.5 \mu\text{m}$  in order to provide data for the design of GaInAsP lasers and detectors for the  $1.2$  to  $1.6 \mu\text{m}$  fiber optic range, which utilize p-type InP layers. In addition, the spectral dependence of  $\alpha$  between  $1.5$  and  $11 \mu\text{m}$  has been measured to give an indication of the scattering mechanisms involved in the free-carrier absorption.

The samples used in this study were taken from LEC boules doped with Zn or Cd to give room-temperature carrier concentrations ranging from  $1.4 \times 10^{16}$

to  $3.4 \times 10^{18} \text{ cm}^{-3}$ . The samples were oriented so that their broad faces were (110) planes, since chemical polishing of these non-polar planes yields very smooth surfaces. Each sample was lapped to a thickness chosen to give transmission values that were high enough for a good signal-to-noise ratio in the detector circuit but were significantly lower than the reflectivity limit. The samples were chemically-mechanically polished with a dilute bromine-methanol solution and free etched to remove surface damage.

Transmission measurements were made at 300 K with a double-pass prism monochromator. Radiation from an Opperman glower was chopped at 13 Hz and detected with a 1-mm-diameter pyroelectric detector, using a standard lock-in technique. A 1-mm aperture was placed in front of the detector, and the InP sample was placed directly in front of the aperture. Transmission values measured with a single-pass prism monochromator were consistently too high for wavelengths greater than about 5  $\mu\text{m}$ . The effect was caused by radiation in the 1 to 3  $\mu\text{m}$  region, where the intensity from the source is largest, that was scattered through the monochromator. Since the samples are most transparent just beyond the absorption edge at  $\sim 1 \mu\text{m}$ , a large fraction of the scattered radiation reached the detector while only a small fraction of the long wavelength radiation (at the monochromator setting) did so. The double-pass instrument eliminated this problem.

Since the LEC boules were grown in a (111) direction, most samples with (110) faces were prepared from longitudinal slices. Because of the growth striation inhomogeneities described in the previous section, the transmission through some of these samples was found to depend strongly on what region of the sample was placed in front of the detector aperture. In addition,

rotating such samples by 90° could change the transmission by as much as 30%. The values of  $\alpha$  were determined from data for selected samples whose transmission did not vary by more than 2 or 3% with translation or rotation.

The values of  $\alpha$  were again calculated by using the expression  $I/I_0 = [(1-R)^2 \exp(-\alpha x)] / [1-R^2 \exp(-2\alpha x)]$ . At normal incidence, the reflectivity is given by

$$R = \frac{(n-1)^2 + k^2}{(n+1)^2 + k^2},$$

where  $n$  is the refractive index and  $k$  is the extinction coefficient. Since  $k$  can be neglected for InP over the wavelength range studied,  $R \approx (n-1)^2 / (n+1)^2$ . Values for  $R$  as a function of wavelength were calculated from this expression by using the refractive index data of Pettit and Turner.<sup>7</sup>

The hole concentration for each optical sample was calculated from the expression  $p = e/R_H$ , using the values of  $R_H$  measured at 300K by the van der Pauw method; that is, we have assumed a single-carrier model with a Hall factor of 1. (The light hole concentration  $p_{lh}$  and heavy hole concentration  $p_{hh}$  can be approximated if the averaged relaxation times for the light and heavy holes are assumed equal, so that the mobility ratio  $\mu_{hh}/\mu_{lh} = m^*_{lh}/m^*_{hh}$ , and if  $p_{hh}/p_{lh}$  is taken to be  $(m^*_{hh}/m^*_{lh})^{3/2}$ . Using the reported<sup>8</sup> effective mass values  $m^*_{hh} = 0.45 m_0$  and  $m^*_{lh} = 0.12 m_0$ , one obtains  $p_{lh} \approx 0.18 e/R_H$  and  $p_{hh} \approx 1.3 e/R_H$ ).

Figure 11 shows log-log plots of  $\alpha$  vs  $p$  for  $\lambda = 1.5 \mu\text{m}$  and  $\lambda = 10.6 \mu\text{m}$ . The data for the shorter wavelength are consistent with a constant cross section,  $\alpha/p = 2.5 \times 10^{-17} \text{ cm}^2$ . At  $\lambda = 10.6 \mu\text{m}$ ,  $\alpha/p$  increases slightly with increasing carrier concentration, from  $2.6 \times 10^{-16} \text{ cm}^2$  at  $p = 1 \times 10^{16} \text{ cm}^{-3}$  to  $4.3 \times 10^{-16} \text{ cm}^2$  at  $p = 1 \times 10^{18} \text{ cm}^{-3}$ . It should be pointed out that

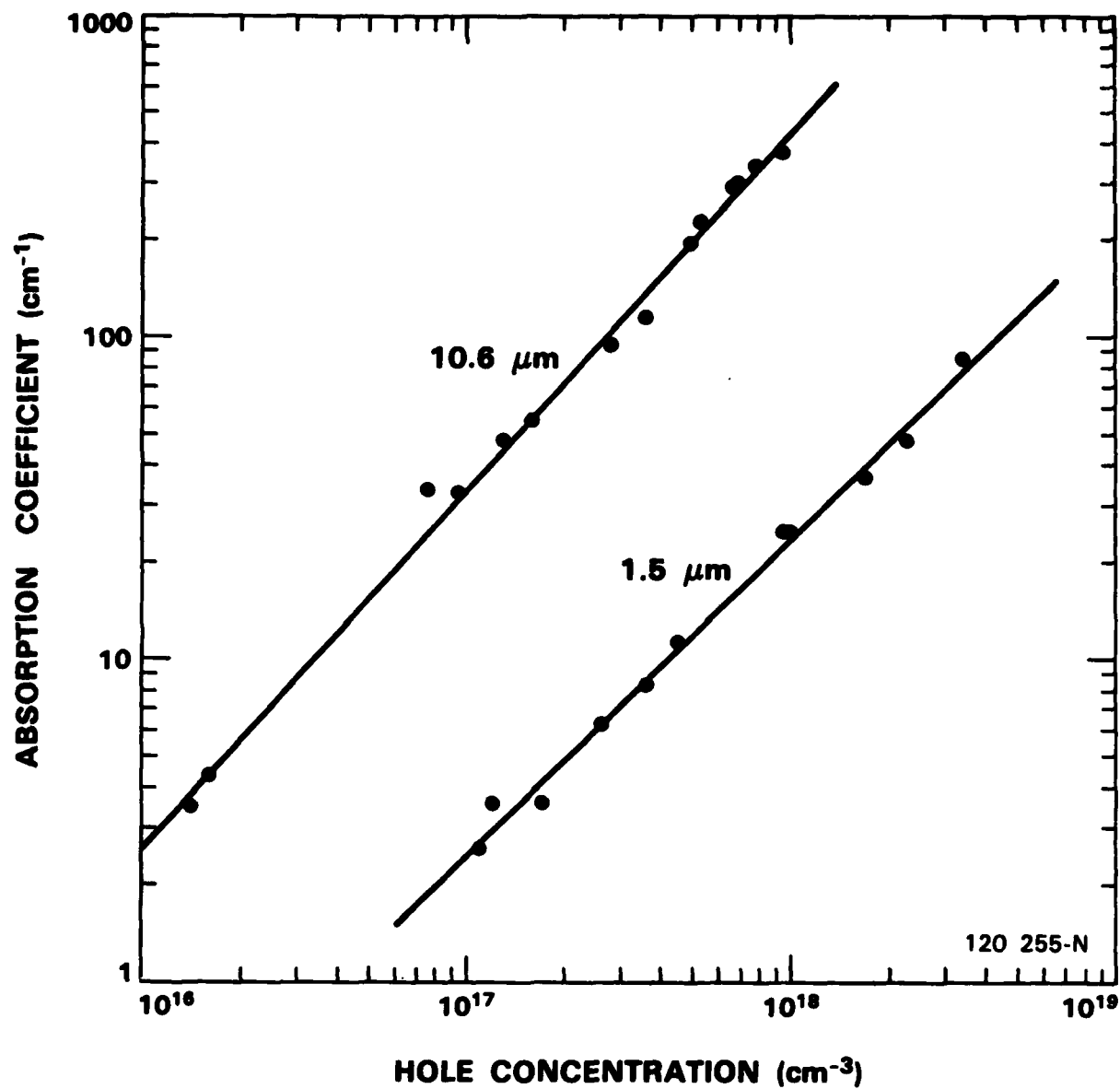


Fig. 11 Absorption coefficients at 1.5 and 10.6  $\mu\text{m}$  vs hole concentration at 300 K for p-type InP samples.

these values of  $\alpha/p$  are considerably lower than those calculated from the data at 10  $\mu\text{m}$  reported by Yamaguchi, et al.<sup>9</sup>

Figure 12 is a log-log plot showing the absorption between 1.5 and 10.5  $\mu\text{m}$  for 4 different carrier concentrations. In each case  $\alpha$  increases monotonically with  $\lambda$ , and the data can be represented fairly well by two straight lines, with the smaller slope at longer wavelengths. Thus the spectra do not exhibit the pronounced structure due to intervalence-band transitions that is observed for p-type samples of most other semiconductors (for example, Ge,<sup>10</sup> GaAs,<sup>11</sup> and AlSb<sup>11</sup>), nor do they have the simple  $\lambda^m$  power dependence that is characteristic of intraband free-carrier absorption. Instead, the InP spectra are very similar in both wavelength dependence and magnitude to the free-carrier absorption spectra observed for p-type GaP by Wiley and DiDomenico.<sup>12</sup> These authors showed theoretically that the special characteristics of the GaP spectra can be attributed to the unusually low spin-orbit splitting in GaP, which is only 0.082 eV.<sup>13</sup> According to their analysis, the absorption of p-type GaP over the wavelength range from 2  $\mu\text{m}$  to the onset of strong lattice absorption at  $\sim 12 \mu\text{m}$  arises from two free-carrier contributions: a weakly structured intervalence-band absorption that generally increases with  $\lambda$ , and a smaller intraband absorption that varies as  $\lambda^{1.7}$ . By adjusting the magnitudes of these contributions, they were able to obtain quite a good fit to the experimental data, which are approximated by two straight lines (although these lines have no direct physical significance). Since the spin-orbit splitting in InP is also very low -- 0.108 eV (Ref. 8) -- it is very probable that the same explanation is applicable in this case.

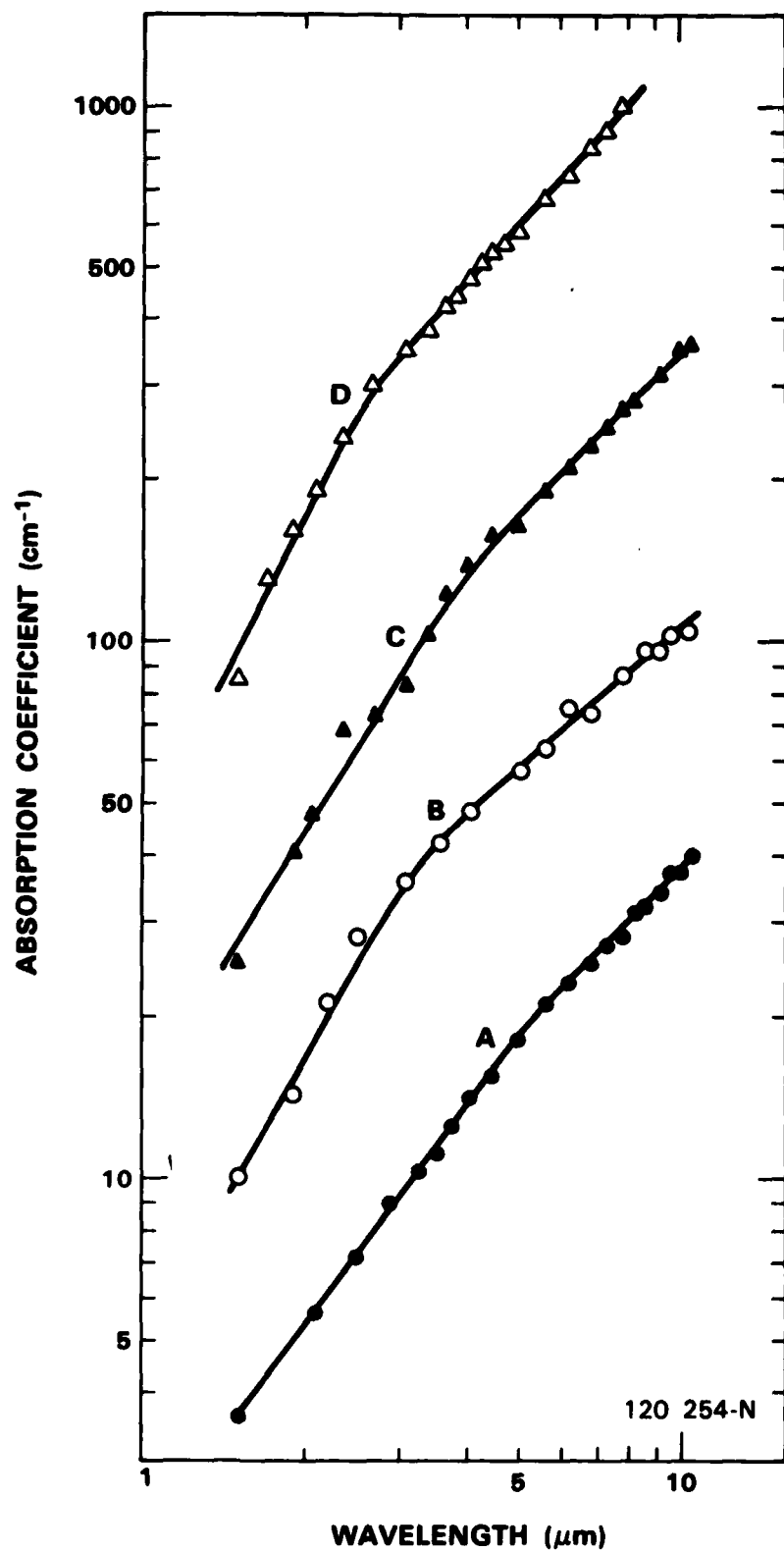


Fig. 12

Absorption coefficient vs wavelength for p-type InP samples with hole concentrations of (A)  $1.2 \times 10^{17} \text{ cm}^{-3}$ , (B)  $3.6 \times 10^{17} \text{ cm}^{-3}$ , (C)  $1.0 \times 10^{18} \text{ cm}^{-3}$ , and (D)  $3.4 \times 10^{18} \text{ cm}^{-3}$ .

#### ACKNOWLEDGEMENTS

The author is grateful to J. V. Pantano, E. J. Delaney and M. S. Taylor for their expert technical assistance and to E. B. Owens for the spark source mass spectrographic analyses.

## REFERENCES

1. W. Walukiewicz, J. Lagowski, L. Jastrzebski, P. Rava, M. Lichtensteiger, C. H. Gatos, and H. C. Gatos, *J. Applied Phys.* 51, 2659 (1980).
2. E. Kubota and K. Sugii, *J. Appl. Phys.* 52, 2983 (1981).
3. A. Huber and N. T. Linh, *J. Cryst. Growth* 29, 80 (1975).
4. J. Matsui, H. Watanabe, and Y. Seki, *J. Crystal Growth*, 46, 563 (1979).
5. G. A. Antypas, in Gallium Arsenide and Related Compounds, St. Louis 1976 (The Institute of Physics, London, 1977), p. 55.
6. C. M. Wolfe and G. E. Stillman, Semiconductors and Semimetals, R. K. Willardson and A. C. Beer, eds. (Academic Press, New York, 1975), Vol. 10, p. 175.
7. G. D. Pettit and W. J. Turner, *J. Appl. Phys.* 36, 2081 (1965).
8. P. Rochon and E. Fertin, *Phys. Rev. B* 12, 5803 (1975).
9. M. Yamaguchi, A. Yamamoto, S. Shinoyama, and H. Sugiura, *J. Appl. Phys.* 53, 633 (1981).
10. A. H. Kahn, *Phys. Rev.* 97, 1647 (1955).
11. R. Braunstein and E. O. Kane, *J. Phys. Chem. Solids* 23, 1423 (1962).
12. J. D. Wiley and M. DiDomenico, Jr., *Phys. Rev. B* 3, 375 (1971).
13. P. J. Dean, G. Kaminsky, and R. B. Zetterstrom, *J. Appl. Phys.* 38, 3551 (1967).

**UNCLASSIFIED**

SECURITY CLASSIFICATION OF THIS PAGE (When Data Entered)